nanomaterials

MDPI

Article

First-Principles Study of Ir_n (n = 3–5) Clusters Adsorbed on Graphene and Hexagonal Boron Nitride: Structural and Magnetic Properties

Mei Ge [1,2], Leiting Chu [1,2], Miaomiao Guo [1,2], Yan Su [3] and Junfeng Zhang [1,2,*]

[1] School of Physics and Information Engineering, Shanxi Normal University, Taiyuan 030031, China; gemei@sxnu.edu.cn (M.G.); chult123@163.com (L.C.); guomm95@163.com (M.G.)
[2] Key Laboratory of Spectral Measurement and Analysis of Shanxi Province, Shanxi Normal University, Taiyuan 030031, China
[3] Key Laboratory of Materials Modification by Laser, Electron, and Ion Beams, Dalian University of Technology, Ministry of Education, Dalian 116024, China; su.yan@dlut.edu.cn
* Correspondence: zhangjf@sxnu.edu.cn; Tel.: +86-13935705526

Abstract: Magnetic clusters have attracted great attention and interest due to their novel electronic properties, and they have potential applications in nanoscale information storage devices and spintronics. The interaction between magnetic clusters and substrates is still one of the challenging research focuses. Here, by using the density functional theory (DFT), we study the structural stability and magnetic properties of iridium clusters (Ir_n, n = 3–5) adsorbed on two-dimensional (2D) substrates, such as graphene and hexagonal boron nitride (*h*BN). We find that the most favorable configurations of free Ir_n clusters change when adsorbed on 2D substrates. In the meantime, the magnetic moments of the most stable Ir_n reduce to 53% (graphene) and 23.6% (*h*BN) compared with those of the free−standing ones. Interestingly, about 12-times enlargement on the magnetic anisotropy energy can be found on *h*BN substrates. These theoretical results indicate that the cluster–substrate interaction has vital effects on the properties of Ir_n clusters.

Keywords: clusters; graphene; hexagonal boron nitride; substrate effect; magnetic property

Citation: Ge, M.; Chu, L.; Guo, M.; Su, Y.; Zhang, J. First-Principles Study of Ir_n (n = 3–5) Clusters Adsorbed on Graphene and Hexagonal Boron Nitride: Structural and Magnetic Properties. *Nanomaterials* **2022**, *12*, 2436. https://doi.org/10.3390/nano12142436

Academic Editor: Rodolphe Antoine

Received: 23 June 2022
Accepted: 14 July 2022
Published: 16 July 2022

1. Introduction

Owing to unexpected electronic and magnetic properties, atomic clusters are promising candidates for technological applications such as catalysis and magnetic storage. They have been becoming gradually more and more attractive in interdisciplinary fields since the 1990s [1–3]. The size and atomic structure-dependent properties of clusters present a huge opportunity for designing cluster-assembled materials and devices. Therefore, determining the ground state structure of a cluster directly by combining experimental and theoretical techniques is vital [1,4].

Magnetic clusters have attracted special attention, especially those composed of transition metals (TM) [5]. Because of the strong spin–orbital coupling (SOC), it is expected that nanostructures containing TM atoms will possess possibly greater magnetic anisotropy energy (MAE), which is a key parameter in nano-information storage devices. Generally, with the increase in the atom number *n*, the geometric structure of clusters will undergo a transition from line models (n = 2–3) to planar models (n = 3–5) and then to three-dimensional configurations (such as a pyramid, octahedron, icosahedron, cube or core-shell model) [6–13]. For instance, owing to the *s(p)-d* hybrid, there is a predominantly icosahedral growth for Fe_{13} and Pd_{13} clusters [14,15]. The electronic and magnetic properties of magnetic clusters highly depend on the atomic size. As the cluster size increases, an odd–even oscillation of vertical ionization potentials occurs in Ir_n (n < 8) and Rh_n (n < 13) clusters [16,17]. The strongly quenched orbital magnetic moment in size-dependent Fe_n (n = 3–20) clusters is

obtained experimentally [14] and then confirmed by DFT calculations [18]. Furthermore, the size effects on magnetic moments have also been observed in Ni_n (n = 10–15) [19,20], Rh_n (n = 2–13) [3,16], Pd_n (n = 2–23, 55, 147) [15], Pt_n (n = 2–20) [21] and Ir_n (n = 1–13) clusters [22].

Generally, clusters can be experimentally prepared by several methods, such as magnetron sputtering [23], laser vaporization [24–26] and chemical vapor deposition (CVD) [27]. Normally, a substrate is necessary for many applications of the clusters. The interaction between the cluster and substrate can affect both the geometric structure and physical properties of a cluster. For instance, under the influence of the cluster–substrate interaction, Fe_n (n = 2–7), (Mn_n (n = 2–7) and Si_n (n = 2–6, 10)) clusters on graphene prefer different growth modes and various orientations [28,29]. Additionally, the electronic and magnetic properties of the substrate can be effectively modulated by the adsorption of clusters [30–33]. When the Mn_5 cluster is absorbed on graphene, the magnetic moment of the Mn_5 cluster is enhanced by 186% because of the electron redistribution [29]. On the contrary, for Fe_n (n = 1, 4–6) clusters, the magnetic moment is reduced by 2–4 μ_B [28]. Furthermore, magnetic clusters can turn into stable nonmagnetic clusters when adsorbed on 2D substrates [33]. Interestingly, a large MAE can be achieved by absorbing clusters on substrates. Among them, Ir_n is a suitable candidate for nano-information storage devices and has been investigated extensively. Hu et al. [34] put an Ir_2 dimer on the double vacancy site of 2D hexagonal boron nitride (*h*BN) and obtained an enlargement in MAE (~126 meV) [35]. Meanwhile, we have also investigated the substrate effect on MAE of Ir_2 and found that MAE depends on the adsorption site and density [36]. However, from our limited knowledge, the interactions between magnetic clusters and substrates are still far from well known, especially on the MAE of larger clusters.

In this paper, by using first-principles calculations, we systematically study the interactions between Ir_n (n = 3–5) clusters and 2D substrates (graphene, *h*BN and germanene) [37]. Different ground state geometric structures of Ir_n and absorption sites of substrates are considered. We first investigate the geometric structures and stabilities with the help of cohesive and detachment energies. Then, we discuss the magnetic properties, including the magnetic moments and MAE, and explore the physics picture with the help of the local density of states and perturbation theory analysis. The present theoretical studies will provide insight into the substrate effect on larger magnetic clusters.

2. Materials and Methods

The structural, magnetic and electronic properties of Ir_n (n = 3–5) clusters adsorbed on 2D materials were studied by first-principles calculations, as implemented in the Vienna Ab-initio Simulation Package (VASP) code [38]. The ion–electron interaction was treated with the projector-augmented plane wave (PAW) potentials [39], and the exchange-correlation potential was described by generalized gradient approximation (GGA) with the Perdew–Burke–Ernzerhof (PBE) functional [40]. The wave functions were expanded in a plane wave basis set with an energy cut-off of 500 eV. The 2D substrates were chosen as 7 × 7 graphene, 7 × 7 *h*BN and 4 × 4 germanene supercells, respectively. To avoid the interaction between two neighboring layers, a vacuum space of 40 Å was added along the Z-direction. A *k*-mesh of 3 × 3 × 1 was used for the Brillouin zone. The atomic structures were fully relaxed without any symmetric constraints, with total energy and force convergence criteria of 10^{-4} eV and 0.01 eV/Å, respectively. For the calculations of the magnetic and electronic properties, the convergence criterion for the total energy was set to 10^{-6} eV, and the SOC effects were considered.

We employed binding energy (E_b, eV), cohesive energy (E_{coh}, eV/atom) and detachment energy (E_{det}, eV) to determine the most energetically favorable configuration of Ir_n/2D. E_b can be used to evaluate the interaction between the Ir_n cluster and the 2D substrate, which is defined as:

$$E_b = E_{Ir_n} + E_{2D} - E_{Ir_n/2D} \quad (1)$$

where E_{Ir_n}, E_{2D} and $E_{Ir_n/2D}$ are the total energies of the free−standing Ir_n cluster, 2D substrate (graphene or *h*BN) and Ir_n/2D hybrid system, respectively. A larger E_b means a stronger interaction between Ir_n and the 2D materials. E_{coh} is the energy gain when isolated Ir atoms are assembled into the Ir_n cluster, which is defined as:

$$E_{coh} = (n \times E_{Ir} - E_{Ir_n})/n \text{ or } E_{coh} = (E_{2D} + n \times E_{Ir} - E_{Ir_n/2D})/n \quad (2)$$

Here, n is the number of Ir atoms of the Ir_n cluster, E_{Ir} is the energy of an isolated Ir atom, E_{Ir_n} is the total energy of the free−standing Ir_n cluster and E_{2D} is the total energy of the 2D substrate, respectively. E_{det} is the energy gain when the Ir_{n-1} cluster is transformed to Ir_n by adding one more Ir atom, which can be used to determine the most favorable cluster size n. For the free−standing cluster Ir_n or that on the 2D substrate, the detachment energy can be defined as:

$$E_{det} = E_{Ir_{n-1}} + E_{Ir} - E_{Ir_n} \text{ or } E_{det} = E_{Ir_{n-1}/2D} + E_{Ir/2D} - E_{Ir_n/2D} - E_{2D} \quad (3)$$

where $E_{Ir_{n-1}/2D}$ and $E_{Ir/2D}$ are the total energies of the Ir_{n-1}/2D and Ir/2D hybrid systems, respectively.

3. Results

3.1. Structural Properties

We investigated the structural, electronic and magnetic properties of the magnetic Ir_n clusters on different 2D substrates and then compared them with the free−standing ones. For the Ir_n (n = 3, 4, 5) clusters, we considered different isomers corresponding to the most stable configuration and the metastable ones. We then put the Ir_n cluster above three kinds of substates: graphene, *h*BN and germanene, respectively. Owing to the stronger interaction between the Ir and Ge atoms, the Ir_n cluster will dissociate and embed into the monolayer germanene, which can induce defected germanene. Taking Ir_3 clusters as the examples, we show the optimized configurations of Ir_3 adsorbed on germanene (see Supplementary Figure S1). Therefore, differently from our previous work in which the favorite adsorption site for the Ir_2 cluster was the single vacancy of germanene [36], we mainly discussed the graphene and *h*BN substrates. Three kinds of absorption sites have been considered: on the top of an atom (T), on the top of a C-C (B-N) bond (B) and on the top of a hexagonal-ring-center (H). Accordingly, the Ir_n cluster absorbed on the 2D substrate is named Ir_{nm}/2D-T (or B, H; see Figure 1), where n = 3, 4, 5 is the number of Ir atoms, m = a, b, c labels different isomers of free−standing Ir_n clusters, 2D is either graphene or *h*BN and T (or B, H) labels the absorption site of the nearest Ir atom.

As shown in Figure 1a,b, there are two relative stable configurations for the free-standing Ir_3 cluster: the line model (Ir_{3a}) and the triangle model (Ir_{3b}). Hereafter, we set the energy of the most stable configuration as zero and ΔE as the energy difference between the most stable and metastable configuration, as listed in Table 1. Ir_{3a} is more stable than Ir_{3b}, with an energy difference of 0.124 eV. Ir_{3a} has an average bond length of 2.181 Å. These results are consistent with most previous PBE calculations [22,41] and PW91 calculations [33]. However, when absorbed on graphene or the *h*BN substrate, the Ir_3 cluster prefers the triangle model because of the substrate effect (see Figure 1c–h), which is similar to the Si_3 cluster absorbed on the graphene substrate [42]. ΔE is 0.159 eV (on graphene) and 0.268 eV (on *h*BN), respectively. For the graphene substrate, the most stable configuration is the Ir_{3b}/graphene-H (Figure 1c) hybrid system, in which the Ir_3 plane is perpendicular to the graphene sheet, the innermost Ir atom is located at the H site with a *d* (distance between the Ir atom and the substrate) of 1.771 Å and the other two Ir atoms are located at the B site. As opposed to Ir_{3b}/graphene-H, the most stable configuration is Ir_{3b}/*h*BN-TT (Figure 1f), in which the plane of the Ir_3 cluster has a tilt angle of 76.5° with a horizontal *h*BN sheet. Compared with Ir_{3b}/graphene-H, there is an inversion for the triangle model, in which two nearer absorbed Ir atoms form chemical bonds with N atoms

with a *d* of 2.248 Å. Owing to two Ir-N bonds, Ir_{3b}/*h*BN-TT has an E_b of 5.583 eV, which is higher than that of Ir_{3a}/graphene-H (5.352 eV).

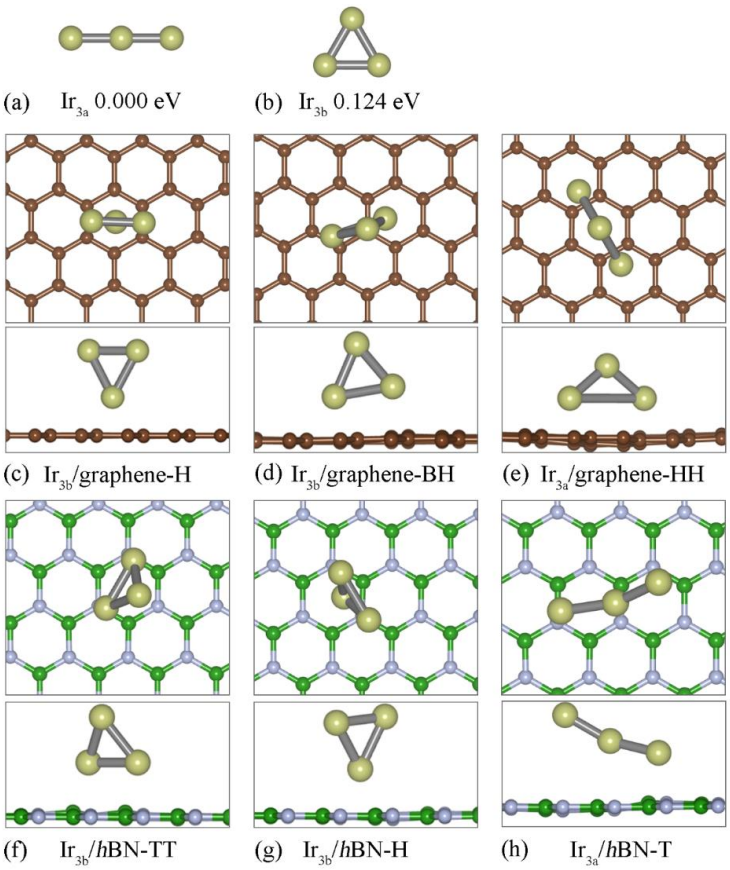

Figure 1. Atomic structures of the (**a**) Ir_{3a} (line model) and (**b**) Ir_{3b} (triangle model) clusters. Top and side view of the three relative stable atomic structures of the Ir_3 cluster adsorbed on the graphene (**c**–**e**) and *h*BN (**f**–**h**) substrate, respectively. The Ir, C, B and N atoms are labeled with golden, brown, green and gray balls, respectively.

Figure 2 shows three kinds of relative stable Ir_4 configurations for the free−standing clusters, and those absorbed onto the graphene and *h*BN substrates, respectively. For the free−standing Ir_4 clusters, the square planar (Ir_{4a}, Figure 2a) is the most favorable configuration and has an average bond length of 2.338 Å. The most stable configuration and structure parameters are consistent with those in the previous report [22]. Unlike the Ir_3 cluster, the most stable configurations of Ir_{4a} remain unchanged on both the graphene and *h*BN substrate, along with a slight band angle deformation when they are adsorbed onto *h*BN. Figure 2e,h indicate that the metastable Ir_4 on either the graphene or *h*BN is still a square planar configuration. The difference is that that are two Ir atoms bonded with the substrate in the most stable configuration, but there is only one in the metastable structure. Therefore, ΔE decreases from 1.251 eV (free−standing Ir_{4b}) to 0.411 (Ir_{4a}/*h*BN-T) and 0.093 eV (Ir_{4a}/graphene-T), respectively. Similar to Ir_{3b}/*h*BN-TT, for Ir_{4a}/*h*BN-TT (Figure 2g), the Ir_{4a} cluster plane has a tilt angle of 75.1° with the *h*BN sheet because of the strong Ir-N interactions. As shown in Table 1, Ir_4/*h*BN has a higher E_b compared with Ir_4/graphene, which indicates a stronger interaction between the cluster and the substrate. Note that, because the configuration of the Ir_n cluster in Ir_n-2D may be different, a higher E_b indicates a stronger interaction between the cluster and the substrate and does not guarantee a higher stability. For example, as listed in Table 1, Ir_{4c}/*h*BN-TTT (Figure 2i) has a larger E_b, along with a higher total energy.

Table 1. The energy difference between the most stable configuration and its isomer (ΔE, eV), the binding energy (E_b, eV), the minimum distance between the cluster and the substrate (d, Å), the magnetic moment of the clusters (μ, μ_B) and the hybrid system (μ_{tot}, μ_B) and the transferred charge from the cluster to the 2D substrate (δ, e). The negative δ represents the electrons transferring from the cluster to the 2D substrate.

	ΔE	E_b	d	**μ**	μ_{tot}	**δ**
Ir_{3b}/graphene-H	0	5.352	1.771	1.408	1.287	−0.163
Ir_{3b}/graphene-BH	0.159	5.192	2.007	2.385	2.517	−0.221
Ir_{3a}/graphene-HH	0.278	4.950	1.714	1.017	1.083	−0.269
Ir_{3b}/*h*BN-TT	0	5.583	2.248	2.687	2.713	−0.0305
Ir_{3b}/*h*BN-H	0.268	5.315	1.957	2.644	2.702	0.101
Ir_{3a}/*h*BN-T	0.691	4.768	2.253	0.822	0.829	0.107
Ir_{4a}/graphene-BB	0	4.818	2.662	4.929	4.973	−0.245
Ir_{4a}/graphene-T	0.093	4.725	2.080	4.943	4.941	−0.104
Ir_{4b}/graphene-H	0.462	5.607	1.895	0.548	0.259	−0.037
Ir_{4a}/*h*BN-TT	0	5.546	2.363	1.535	1.519	−0.023
Ir_{4a}/*h*BN-T	0.411	5.135	2.241	2.877	2.900	0.010
Ir_{4c}/*h*BN-TTT	0.938	6.722	2.075	0	0	−0.133
Ir_{5a}/graphene-H	0	5.434	1.989	4.516	4.539	−0.173
Ir_{5a}/graphene-TTTT	0.586	4.847	2.374	2.181	2.196	−0.468
Ir_{5b}/graphene-BB	0.645	5.029	2.595	2.452	2.452	−0.170
Ir_{5a}/*h*BN-H	0	5.554	1.736	3.861	3.844	0.093
Ir_{5c}/*h*BN-T	0.103	6.567	2.298	2.377	2.358	0
Ir_{5b}/*h*BN-H	0.172	5.622	1.742	3.940	3.933	0.067

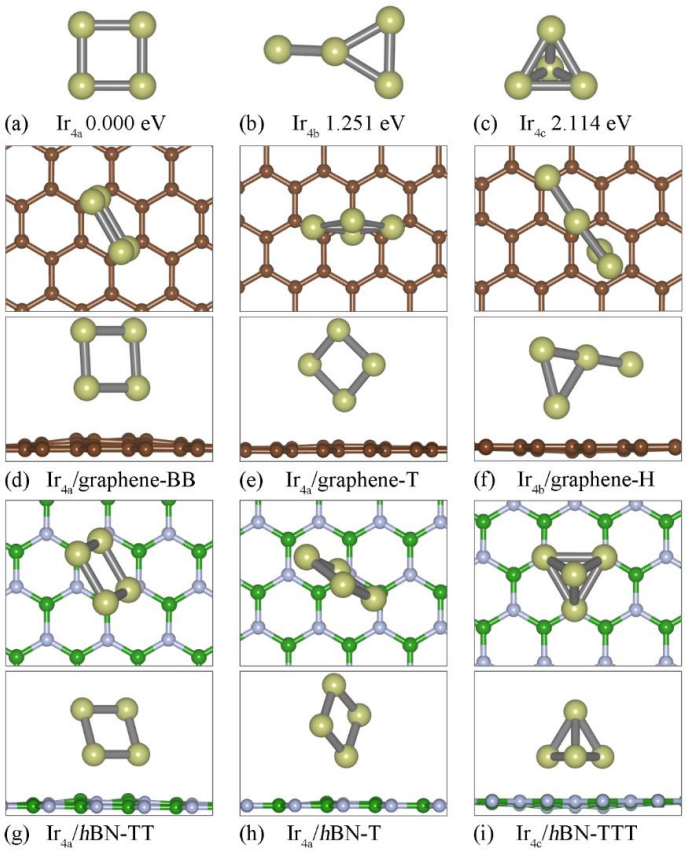

Figure 2. Atomic structures of the (**a**) Ir_{4a} (square planar model), (**b**) Ir_{4b} (a triangle configuration adding the fourth atom attached with the vertex of the triangle) and (**c**) Ir_{4c} (tetrahedral model) clusters. Top and side view of the three relative stable atomic structures of the Ir_4 cluster adsorbed on the graphene (**d**–**f**) and *h*BN (**g**–**i**) substrate, respectively.

The free−standing Ir_5 isomers are listed in Figure 3a–c, in which Ir_{5a} (square pyramid model) is the most stable configuration, and the metastable ones are Ir_{5b} (square adding a co-plane triangle model, with an ΔE of 0.24 eV) and Ir_{5c} (triangular bipyramid model, with an ΔE of 1.117 eV), respectively. When it is absorbed on the 2D substrates, the square pyramid Ir_{5a} is still the most stable. A previous theoretical calculation also suggested that the square pyramid model of Ir_5 is more stable for both free−standing clusters [22,33,41] or on the monolayer graphene [43]. As shown in Figure 3d,g, the bottommost Ir atom of the cluster is located at the H site of the graphene (*h*BN) with a *d* of 1.989 (1.736) Å. Ir_{5c}/*h*BN-T is metastable owing to its higher E_b (6.567 eV), which is larger than that of Ir_{5b}/*h*BN-H (5.622 eV).

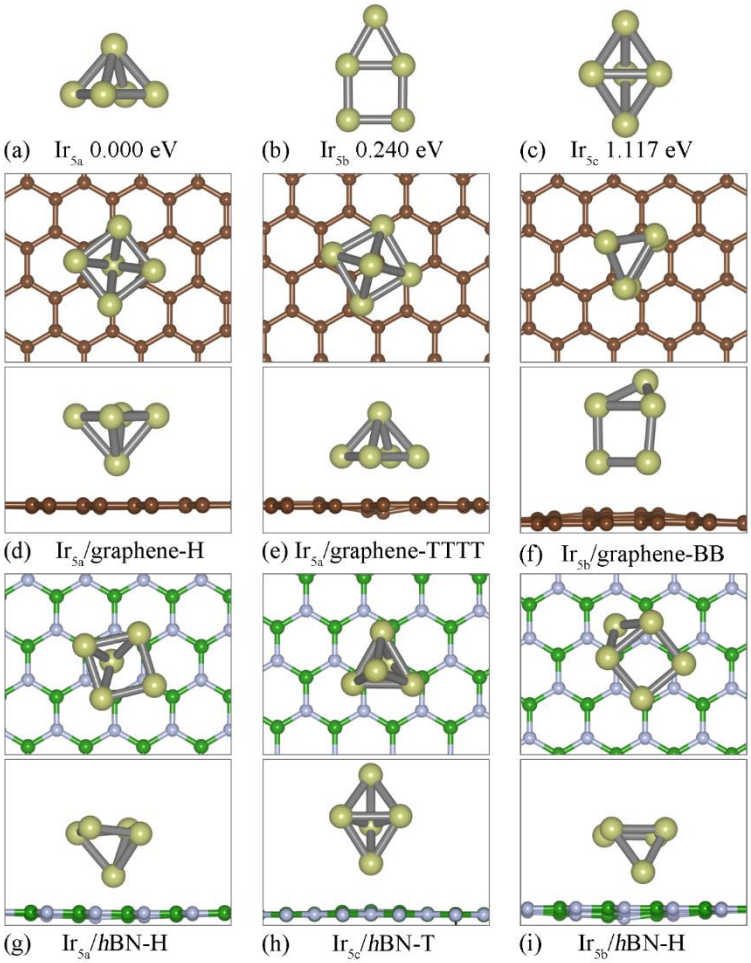

Figure 3. Atomic structures of the three relative stable atomic structures of the Ir_5 clusters for the free-standing (**a**–**c**), graphene ((**d**–**f**), top and side view) and *h*BN ((**g**–**i**), top and side view) substrate, respectively.

We employ E_{coh} and E_{det} to further discuss the favorable Ir_n clusters on the substrates. As shown in Figure 4a, E_{coh} increases with the number of cluster atoms (n) for both the free−standing Ir_n [33] and Ir_n/2D hybrid systems. Compared with the free−standing Ir_n cluster, Ir_n/2D possesses a higher E_{coh}, suggesting that the substrate effect can make the Ir_n cluster energetically stable. The E_{coh} of Ir_5 on graphene (*h*BN) is 5.19 (5.34) eV/atom, which is comparable with that from Ghazi's works [43,44]. As plotted in Figure 4b, for free−standing clusters, that the maximum of E_{det} belongs to the Ir_4 configuration indicates that Ir_4 is the favorite Ir_n cluster. After being absorbed on the substrates (either graphene or *h*BN), Ir_3/2D turns out to be the most stable configuration due to it having the largest E_{det}.

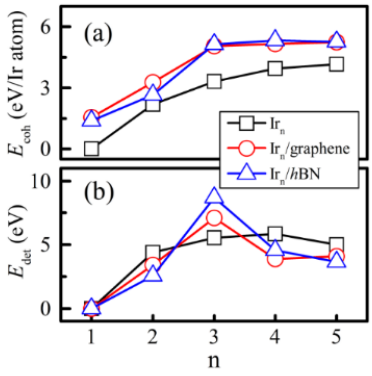

Figure 4. E_{coh} (**a**) and E_{def} (**b**) of the most stable structure for the Ir_n, Ir_n/graphene (*h*BN) clusters (n = 1–5).

3.2. Magnetic Properties

We next discuss the magnetic properties of Ir_n clusters on graphene and *h*BN. By setting different spin directions in Ir_n, we can determine what the magnetic ground state (ferromagnetic or anti-ferromagnetic) is. For all the stable configurations, including the free−standing Ir_n and Ir_n on the substrates, the ferromagnetic ground state is more energetically favorable, as shown in Supplementary Table S1. The total magnetic moments of the free−standing Ir_{3a} and Ir_{3b} are 0.947 μ_B and 2.654 μ_B, respectively. The total magnetic moments of Ir_{4a}, Ir_{4b} and Ir_{4c} are 6.509 μ_B, 3.583 μ_B and 0 μ_B, respectively. These results are consistent with the previous calculations [22,33]. Moreover, the total magnetic moments of Ir_{5a}, Ir_{5b} and Ir_{5c} change to be 5.574 μ_B, 7.641 μ_B and 7.562 μ_B, respectively. As listed in Table 1, except for Ir_{3a}/graphene-HH and Ir_{3b}/*h*BN-TT, the magnetic moments of the Ir_n clusters on the 2D substrates decrease more or less. Compared with the free−standing Ir_n cluster, the magnetic moments of the most stable Ir_n clusters adsorbed onto the substrates were reduced to 53% (Ir_{3b}/graphene-H) and 23.6% (Ir_{4a}/*h*BN-TT), respectively. Furthermore, for metastable Ir_{4b}/graphene-H, the magnetic moment of the Ir_{4b} cluster is only 0.548 μ_B (84.7% reduction). The variation of the magnetic moment caused by the substrate effect or adsorption site can be understood by the charge transfer between the cluster and the 2D sheet.

Table 1 lists the charge transfer (d) between Ir_n and the substrates from the Bader analysis [45]. Interface bonds may form between the Ir_n cluster and the substrate due to the electron transferring. Firstly, the magnitude of d on graphene is generally larger than that on *h*BN and relies on the absorption site. Secondly, for the considered Ir_n/graphene, electrons transfer from the Ir_n cluster to the graphene sheet, corresponding to a negative d. On the contrary, the transfer direction depends on the bonded atom number when the clusters are absorbed onto the *h*BN substrate. Specifically, if one Ir atom is attached to the substrate, such as in Ir_{3b}/*h*BN-H (as shown in Figure 1), the charges transfer from *h*BN to Ir_n ($d > 0$). If two or more atoms are attached to the substrate, such as in Ir_{3b}/*h*BN-TT, the transfer direction is reversed ($d < 0$).

The density of states (DOS) of the most stable free−standing Ir_n and Ir_n/2D hybrid systems is shown in Figure 5. Generally speaking, the DOS of the Ir_n cluster is perturbed due to the substrate effect. The substrate effect can be divided into two parts: energy level repulsion and charge transfer. From the DFT calculations, the projected DOS indicated that d_{xz} states are induced from the energy level repulsion between the $d_z{}^2$ states of Ir_n and the p_z of C (N) atoms. Meanwhile, the energy level repulsion shifts the states and increases or decreases the magnetic moments of Ir_n. Taking Ir_3 as an example, the magnetic moment of Ir_{3b} (2.654 mB) is increased to 2.687 μ_B on *h*BN but decreased to 1.408 μ_B on graphene. Similar changes can also be found for the Ir_4 and Ir_5 clusters (see Table 1). The charge transfer can be quantitatively characterized by the Bader analysis (Table 1) and qualitatively characterized by the Charge Density Difference (CDD). The CDD in Figure 6 demonstrates that charge redistribution takes place at both the interface region and the

Ir_n cluster. Note that, differently from other Ir_n/2D hybrid systems, the electrons in the Ir_{5a}/*h*BN-H structure transfer from *h*BN to Ir atoms, as listed in Table 1. Accordingly, positive charge density dominates the interface region in Figure 6f.

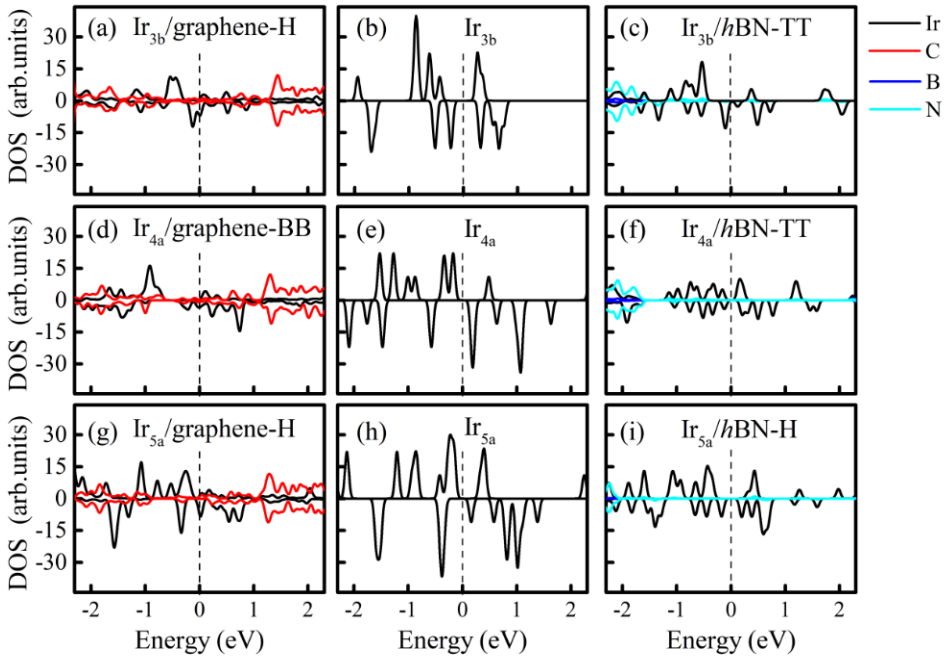

Figure 5. DOS for free standing Ir_n clusters (**b**,**e**,**h**) and Ir_n/graphene (**a**,**d**,**g**) and Ir_n/*h*BN (**c**,**f**,**i**) hybrid systems. Contributions of Ir, C, B and N atoms are highlighted in black, red, blue and cyan, respectively.

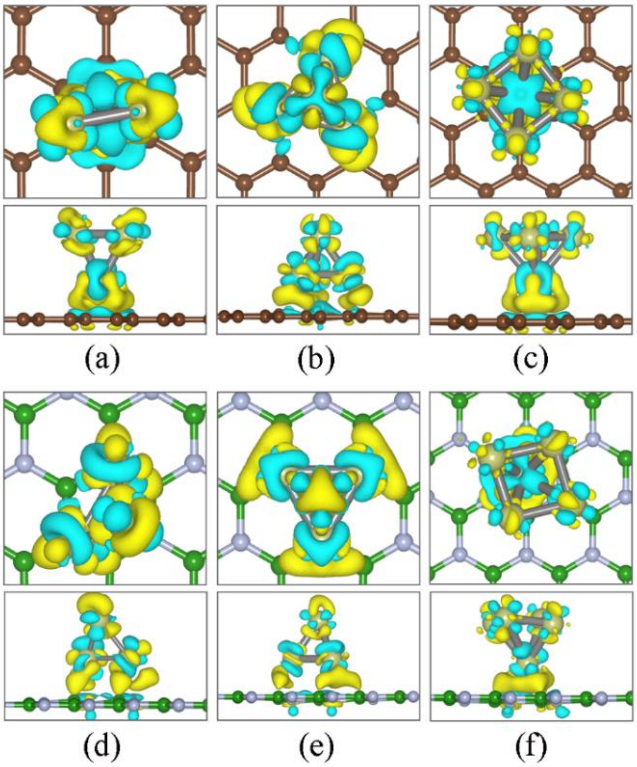

Figure 6. CDD of the most stable structure of Ir_3 to Ir_5 adsorbed on graphene (**a**–**c**) and *h*BN (**d**–**f**). Every figure shows the top and side views of CDD, respectively. Yellow and blue isosurfaces represent positive and negative charge densities. The isosurface is set at 0.005 e $Å^{-3}$.

Finally, we discuss the substrate effect on the magnetic anisotropy energy (MAE) of the Ir_n clusters. MAE is defined as the energy difference between different easy axes (parallel (//) and perpendicular ($\perp$) to the 2D substrate) per Ir atom, i.e., MAE (in meV/Ir atom) = $E_{//} - E_{\perp}$. The MAE values of the free−standing Ir_{3b}, Ir_{4a} and Ir_{5a} are 11.57, 10.05 and 32.43 meV, respectively, which are consistent with previous theoretical calculations [22]. However, owing to the slight structural difference, the MAE of the free−standing Ir_{4b} (9.32 meV) is lower than that yielded from Ge's calculation (40.26 meV) [41]. Figure 7 plots the MAE of the free−standing Ir_n clusters, Ir_n/graphene and Ir_n/*h*BN. Clearly, with the increase in n (from 3 to 5), the Ir_n clusters experience an easy-axis direction change. More importantly, under the influence of the substrate effect, the MAE is enlarged by about 4 times for the Ir_{3b}/graphene and by 12 times for the Ir_{4a}/graphene.

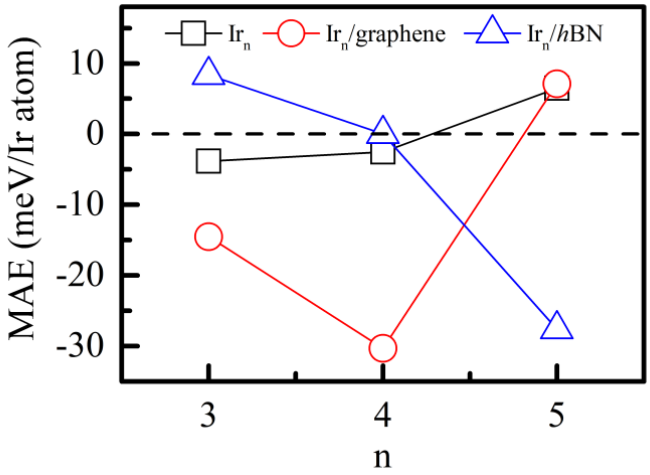

Figure 7. The MAE of the most stable free−standing Ir_n and Ir_n/2D systems (n = 3–5), respectively. The zero MAE is labeled by a dashed line.

MAE can be understood with the help of the second-order perturbation approach [46], which is defined as:

$$\mathrm{MAE} = \xi^2 \sum_{\mathrm{U,O}} \frac{|<\mathrm{O}|l_z|\mathrm{U}>|^2 - |<\mathrm{O}|l_x|\mathrm{U}>|^2}{E_\mathrm{U} - E_\mathrm{O}} \quad (4)$$

where ξ is the SOC constant, O (U) stands for the occupied (unoccupied) states, E_O (E_U) stands for the corresponding energy eigenvalues and l_z (l_x) is the orbital angular momentum operator. As described by Equation (4), the coupling spin orbital matrix element difference, i.e., $|<O|l_z|U>|^2 - |<O|l_x|U>|^2$, contributes to the value of MAE, including different coupling orbitals and various coupling factors. Figure 8 shows the *d* orbital-resolved MAE of the free−standing Ir_n cluster and Ir_n/graphene (Ir_n/*h*BN). As shown in Figure 8b, the main contribution of the free−standing Ir_{3b} cluster to the MAE comes from the matrix element difference between the d_{xz} and $d_z{}^2$ orbitals. However, Figure 8a,c indicate that the main contributions on the substrate changed to d_{xy} and $d_x{}^2{}_{-y}{}^2$ orbitals for both the *h*BN and graphene, owing to the $d_z{}^2$-to-d_{xy} orbitals transition, as discussed above. For Ir_{4a}, Figure 8e (free−standing) and Figure 8f (Ir_{4a}/*h*BN) suggested that the interaction between d_{xz} and d_{xy} is the main contribution for MAE, which results in a smaller MAE. In Ir_{4a}/graphene, we found that the *d* orbital is closer to the Fermi level, resulting in a higher MAE. Finally, the interactions between $d_x{}^2{}_{-y}{}^2$ and d_{xz} (d_{xy}) determine the MAEs of the free−standing (on substrates) Ir_{5a} clusters. The positive (negative) contributions given by the matrix element difference between different orbitals and coupling factors result in different MAE values, as discussed in reference [46].

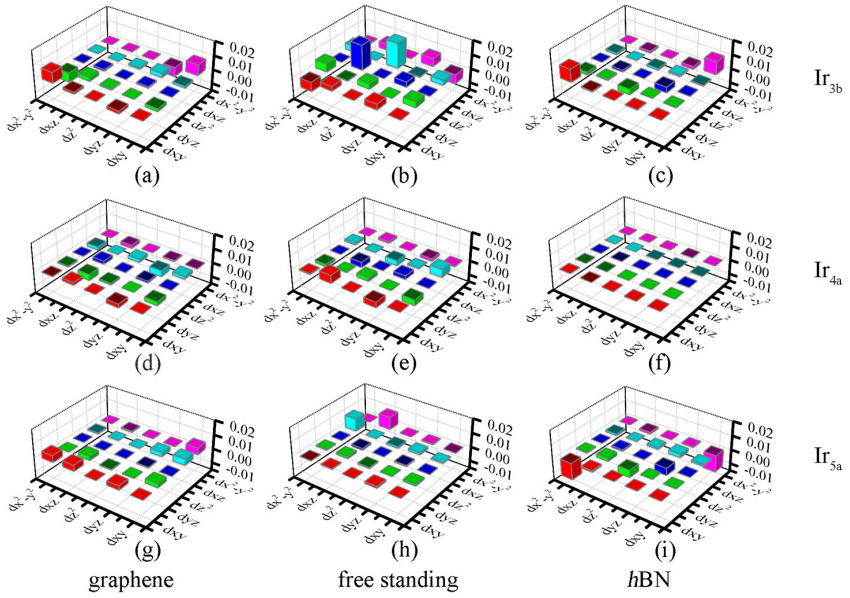

Figure 8. The angular momentum operator matrix of the *d* orbital of the most stable structure: (**a**) Ir_{3b}/graphene-H, (**b**) free−standing Ir_{3b}, (**c**) Ir_{3b}/*h*BN-TT, (**d**) Ir_{4a}/graphene-BB, (**e**) free−standing Ir_{4a}, (**f**) Ir_{4a}/*h*BN-TT, (**g**) Ir_{5a}/graphene-H, (**h**) free−standing Ir_{5a} and (**i**) Ir_{5a}/*h*BN-H. The units of the coordinates are eV.

4. Conclusions

In conclusion, the structural and magnetic properties of Ir_n (n = 3–5) clusters adsorbed on 2D substrates (graphene and *h*BN) were systematically investigated using the DFT method. The calculated results show that, after the structure relaxation, the stability order of Ir_n may change on 2D substrates. The detachment energies suggest that, for the free−standing Ir_n, the most favorite cluster is the one of n = 3. After being absorbed on 2D substrates, the most stable cluster changes to n = 4. The magnetic moments of Ir_n generally decrease owing to the charge transfer between the Ir_n and the substrates, which depends on the substrate type and adsorption site. The MAE of the Ir_n cluster can be enlarged by 12 times for Ir_{4a}/graphene, which is understood with the help of the second-order perturbation approach.

Supplementary Materials: The following supporting information can be downloaded at: https://www.mdpi.com/article/10.3390/nano12142436/s1, Figure S1: Three optimized configurations of Ir_3 on Germanene; Table S1: The relative energies (in meV) of ferromagnetic (FM) and antiferromagnetic (AFM) states for the free−standing Ir_n and Ir_n on graphene and *h*BN substrates. We set the energy of FM (E_{FM}) state as zero.

Author Contributions: M.G. (Mei Ge): conceptualization, writing—review and editing, funding acquisition; L.C.: writing—original draft preparation; M.G. (Miaomiao Guo): designing and performing the DFT calculations; Y.S.: resources; J.Z.: conceptualization, project administration, funding acquisition. All authors have read and agreed to the published version of the manuscript.

Funding: This research was funded by the National Natural Science Foundation of China, grant number 12074235; the Natural Science Foundation of Shanxi Province, grant number 202103021223252; and the Project for Graduate Research Innovation of Shanxi Normal University of China, grant number 2019XSY020.

Institutional Review Board Statement: Not applicable.

Informed Consent Statement: Not applicable.

Data Availability Statement: Not applicable.

Conflicts of Interest: The authors declare no conflict of interest.

References

1. Douglass, D.C.; Bucher, J.P.; Bloomfield, L.A. Magnetic studies of free nonferromagnetic clusters. *Phys. Rev. B* **1992**, *45*, 6341–6344. [CrossRef] [PubMed]
2. Cox, A.J.; Louderback, J.G.; Bloomfield, L.A. Experimental observation of magnetism in rhodium clusters. *Phys. Rev. Lett.* **1993**, *71*, 923–926. [CrossRef] [PubMed]
3. Cox, A.J.; Louderback, J.G.; Apsel, S.E.; Bloomfield, L.A. Magnetism in 4d-transition metal clusters. *Phys. Rev. B* **1994**, *49*, 12295–12298. [CrossRef] [PubMed]
4. Knight, W.D.; Clemenger, K.; de Heer, W.A.; Saunders, W.A.; Chou, M.Y.; Cohen, M.L. Electronic Shell Structure and Abundances of Sodium Clusters. *Phys. Rev. Lett.* **1984**, *52*, 2141–2143. [CrossRef]
5. Chaves, A.S.; Piotrowski, M.J.; Da Silva, J.L.F. Evolution of the structural, energetic, and electronic properties of the 3d, 4d, and 5d transition-metal clusters (30 TMn systems for n = 2–15): A density functional theory investigation. *Phys. Chem. Chem. Phys.* **2017**, *19*, 15484–15502. [CrossRef] [PubMed]
6. Gaston, N.; Schwerdtfeger, P. From the van der Waals dimer to the solid state of mercury with relativisticab initioand density functional theory. *Phys. Rev. B* **2006**, *74*, 024105. [CrossRef]
7. Song, W.; Lu, W.-C.; Wang, C.Z.; Ho, K.M. Magnetic and electronic properties of the nickel clusters Ni_n ($n \leq 30$). *Comput. Theor. Chem.* **2011**, *978*, 41–46. [CrossRef]
8. Ruiz-Díaz, P.; Ricardo-Chávez, J.L.; Dorantes-Dávila, J.; Pastor, G.M. Magnetism of small Cr clusters: Interplay between structure, magnetic order, and electron correlations. *Phys. Rev. B* **2010**, *81*, 224431. [CrossRef]
9. Yuan, H.K.; Chen, H.; Ahmed, A.S.; Zhang, J.F. Density-functional study of Sc_n (n = 2–16) clusters: Lowest-energy structures, electronic structure, and magnetism. *Phys. Rev. B* **2006**, *74*, 144434. [CrossRef]
10. Datta, S.; Kabir, M.; Saha-Dasgupta, T. *Ab initio* study of structural stability of small 3d late transition metal clusters: Interplay of magnetization and hybridization. *Phys. Rev. B* **2011**, *84*, 075429. [CrossRef]
11. Du, J.; Sun, X.; Chen, J.; Jiang, G. A Theoretical Study on Small Iridium Clusters: Structural Evolution, Electronic and Magnetic Properties, and Reactivity Predictors. *J. Phys. Chem. A* **2010**, *114*, 12825–12833. [CrossRef] [PubMed]
12. Guo, P.; Zheng, J.-M.; Zhao, P.; Zheng, L.-L.; Ren, Z.-Y. The relativistic density functional investigations on geometries, electronic and magnetic properties of Ir_n (n = 1–13) clusters. *Chin. Phys. B* **2010**, *19*, 083601.
13. Ilgaz Aysan, I.; Gorkan, T.; Ozdemir, I.; Kadioglu, Y.; Gokoglu, G.; Akturk, E. Electronic structure, cohesive and magnetic properties of iridium oxide clusters adsorbed on graphene. *J. Mol. Graph. Model.* **2020**, *101*, 107726. [CrossRef]
14. Niemeyer, M.; Hirsch, K.; Zamudio-Bayer, V.; Langenberg, A.; Vogel, M.; Kossick, M.; Ebrecht, C.; Egashira, K.; Terasaki, A.; Moller, T.; et al. Spin coupling and orbital angular momentum quenching in free iron clusters. *Phys. Rev. Lett.* **2012**, *108*, 057201. [CrossRef]
15. Kumar, V.; Kawazoe, Y. Icosahedral growth, magnetic behavior, and adsorbate-induced metal-nonmetal transition in palladium clusters. *Phys. Rev. B* **2002**, *66*, 144413. [CrossRef]
16. De Oliveira, A.Z.; Jorge, F.E. Structural, electronic, electrical, and magnetic properties of Rh ($1 \leq n \leq 13$) clusters. *Comput. Theor. Chem.* **2020**, *1177*, 112765. [CrossRef]
17. Jorge, F.E.; da Costa Venâncio, J.R. Structure, stability, catalytic activity, and polarizabilities of small iridium clusters. *Chin. Phys. B* **2018**, *27*, 063102. [CrossRef]
18. Yuan, H.K.; Chen, H.; Kuang, A.L.; Tian, C.L.; Wang, J.Z. The spin and orbital moment of Fe(n) (n = 2–20) clusters. *J. Chem. Phys.* **2013**, *139*, 034314. [CrossRef] [PubMed]
19. Lee, H.W.; Chang, C.M.; Hsing, C.R. Puzzle of magnetic moments of Ni clusters revisited using quantum Monte Carlo method. *J. Chem. Phys.* **2017**, *146*, 084313. [CrossRef]
20. Langenberg, A.; Hirsch, K.; Ławicki, A.; Zamudio-Bayer, V.; Niemeyer, M.; Chmiela, P.; Langbehn, B.; Terasaki, A.; Issendorff, B.V.; Lau, J.T. Spin and orbital magnetic moments of size-selected iron, cobalt, and nickel clusters. *Phys. Rev. B* **2014**, *90*, 184420. [CrossRef]
21. Kumar, V.; Kawazoe, Y. Evolution of atomic and electronic structure of Pt clusters: Planar, layered, pyramidal, cage, cubic, and octahedral growth. *Phys. Rev. B* **2008**, *77*, 205418. [CrossRef]
22. Liang, X.; Wu, X.; Huang, X.; Su, Y.; Hu, J.; Zhao, J. Magnetic Anisotropy of Small Ir_n Clusters (n = 2–5). *J. Cluster. Sci.* **2016**, *27*, 935–946. [CrossRef]
23. Bernareggi, M.; Chiarello, G.L.; West, G.; Ratova, M.; Ferretti, A.M.; Kelly, P.; Selli, E. Cu and Pt clusters deposition on TiO_2 powders by DC magnetron sputtering for photocatalytic hydrogen production. *Catal. Today* **2019**, *326*, 15–21. [CrossRef]
24. Huang, X.; Lu, S.-J.; Liang, X.; Su, Y.; Sai, L.; Zhang, Z.-G.; Zhao, J.; Xu, H.-G.; Zheng, W. Structures and Electronic Properties of V_3Si_n- (n = 3–14) Clusters: A Combined Ab Initio and Experimental Study. *J. Phys. Chem. C* **2015**, *119*, 10987–10994. [CrossRef]
25. Liang, X.-Q.; Deng, X.-J.; Lu, S.-J.; Huang, X.-M.; Zhao, J.-J.; Xu, H.-G.; Zheng, W.-J.; Zeng, X. Probing Structural, Electronic, and Magnetic Properties of Iron-Doped Semiconductor Clusters $Fe_2Ge_n^{-/0}$ (n = 3–12) via Joint Photoelectron Spectroscopy and Density Functional Study. *J. Phys. Chem. C* **2017**, *121*, 7037–7046. [CrossRef]
26. Huang, X.; Xu, H.G.; Lu, S.; Su, Y.; King, R.B.; Zhao, J.; Zheng, W. Discovery of a silicon-based ferrimagnetic wheel structure in V_xSi_{12} (x = 1–3) clusters: Photoelectron spectroscopy and density functional theory investigation. *Nanoscale* **2014**, *6*, 14617–14621. [CrossRef]

27. Barker, B.A.; Bradley, A.J.; Ugeda, M.M.; Coh, S.; Zettl, A.; Crommie, M.F.; Louie, S.G.; Cohen, M.L. Geometry and electronic structure of iridium adsorbed on graphene. *Phys. Rev. B* **2019**, *99*, 075431. [CrossRef]
28. Liu, X.; Wang, C.Z.; Lin, H.Q.; Hupalo, M.; Thiel, P.A.; Ho, K.M.; Tringides, M.C. Structures and magnetic properties of Fe clusters on graphene. *Phys. Rev. B* **2014**, *90*, 155444. [CrossRef]
29. Liu, X.; Wang, C.-Z. Growth mode and structures of magnetic Mn clusters on graphene. *RSC Adv.* **2016**, *6*, 64595–64604. [CrossRef]
30. Cui, H.; Jia, P. Doping effect of small Rh_n (n = 1–4) clusters on the geometric and electronic behaviors of MoS_2 monolayer: A first-principles study. *Appl. Surf. Sci.* **2020**, *526*, 146659. [CrossRef]
31. Ju, W.; Li, T.; Su, X.; Li, H.; Li, X.; Ma, D. Au cluster adsorption on perfect and defective MoS_2 monolayers: Structural and electronic properties. *Phys. Chem. Chem. Phys.* **2017**, *19*, 20735–20748. [CrossRef] [PubMed]
32. Wang, Y.; Su, Y.; Kang, L. Stability and nucleation of Ir_n (n = 1–5) clusters on different γ-Al_2O_3 surfaces: A density functional theory study. *Phys. Lett. A* **2016**, *380*, 718–725. [CrossRef]
33. Chen, Y.; Huo, M.; Chen, T.; Li, Q.; Sun, Z.; Song, L. The properties of Ir_n (n = 2–10) clusters and their nucleation on gamma-Al_2O_3 and MgO surfaces: From ab initio studies. *Phys. Chem. Chem. Phys.* **2015**, *17*, 1680–1687. [CrossRef] [PubMed]
34. Li, J.; Wang, H.; Hu, J.; Wu, R.Q. Search for giant magnetic anisotropy in transition-metal dimers on defected hexagonal boron nitride sheet. *J. Chem. Phys.* **2016**, *144*, 204704. [CrossRef]
35. Xu, M.; Liang, T.; Shi, M.; Chen, H. Graphene-like two-dimensional materials. *Chem. Rev.* **2013**, *113*, 3766–3798. [CrossRef]
36. Guo, M.; Liang, X.; Wang, H.; Zhang, J. Magnetic anisotropy of iridium dimers on two-dimensional materials. *Phys. Chem. Chem. Phys.* **2020**, *22*, 238–244. [CrossRef]
37. Cahangirov, S.; Topsakal, M.; Aktürk, E.; Şahin, H.; Ciraci, S. Two-and one-dimensional honeycomb structures of silicon and germanium. *Phy. Rev. Lett.* **2009**, *102*, 236804. [CrossRef]
38. Kresse, G.; Furthmuller, J. Efficient iterative schemes for ab initio total-energy calculations using a plane-wave basis set. *Phys. Rev. B* **1996**, *54*, 11169. [CrossRef]
39. Kresse, G.; Joubert, D. From ultrasoft pseudopotentials to the projector augmented-wave method. *Phys. Rev. B* **1999**, *59*, 1758–1775. [CrossRef]
40. Perdew, J.P.; Burke, K.; Ernzerhof, M. Generalized Gradient Approximation Made Simple. *Phys. Rev. Lett.* **1996**, *77*, 3865. [CrossRef]
41. Ge, G.-X.; Yan, H.-X.; Yang, J.-M.; Zhou, L.; Wan, J.-G.; Zhao, J.-J.; Wang, G.-H. Manipulation of magnetic anisotropy in Ir_{n+1} clusters by Co atom. *Phys. A* **2016**, *453*, 194–202. [CrossRef]
42. Yong, Y.; Hao, X.; Li, C.; Li, X.; Li, T.; Cui, H.; Lv, S. Density functional studies of small silicon clusters adsorbed on graphene. *RSC Adv.* **2015**, *5*, 38680–38689. [CrossRef]
43. Ostad, F.Z.; Ghazi, M.E.; Javan, M.; Izadifard, M. DFT study of Pt_n, Pd_n, and Ir_n (n = 5, 6) clusters adsorbed on graphene: Structural and electronic properties. *Phys. B* **2019**, *575*, 411678. [CrossRef]
44. Zargari, F.; Javan, M.; Ghazi, M.E.; Izadifard, M. Graphene-like boron nitride supported Ir_n, Pd_n, and Pt_n (n = 5, 6) clusters: A DFT study. *Diam. Relat. Mater.* **2020**, *110*, 108110. [CrossRef]
45. Tang, W.; Sanville, E.; Henkelman, G. A grid-based Bader analysis algorithm without lattice bias. *J. Phys. Condens. Matter* **2009**, *21*, 084204. [CrossRef] [PubMed]
46. Wang, D.S.; Wu, R.; Freeman, A.J. First-principles theory of surface magnetocrystalline anisotropy and the diatomic-pair model. *Phys. Rev. B* **1993**, *47*, 14932–14947. [CrossRef]